Simulation of electrohydrodynamic instability near ion-selective membranes

By C. L. Druzgalski, M. B. Andersen AND A. Mani

1. Motivation and objectives

The passage of an electrical current across the interface of an electrolyte and an ion-selective membrane leads to concentration polarization, i.e., depletion and enrichment of ions in the electrolyte solution (Levich & Spalding 1962). The depletion effect has been utilized for more than half a century in various notable technologies such as electrodialysis (Probstein 1994).

A major outstanding issue is the understanding of ion transfer from the solution into the ion-selective membrane at currents above the classical diffusion limit (Levich & Spalding 1962). The classical test system consists of a quiescent viscous concentration polarization layer (CPL) between a well-stirred reservoir of fixed concentration and an ideal ion-selective membrane. In this problem there is no imposed flow and the problem is homogeneous in the direction tangential to the membrane plates. As the applied potential difference across the system is increased from its equilibrium value, the resulting current displays an initial linear ohmic response. However, as the ion concentration in the diffusion layer drops with the increasing potential difference, the electrical resistance increases. In the limit of an infinite potential difference, the concentration at the ion selective membrane approaches zero and the current asymptotically approaches the limiting current I_{lim}. For a symmetric binary electrolyte

$$I_{\mathrm{lim}} = 2zeD\frac{c_0}{L}, \tag{1.1}$$

in which z is the ionic valence, e is the elementary charge, D is the diffusion constant, c_0 is the reservoir concentration and L is the surface-to-reservoir width (Levich & Spalding 1962). In the experiments, however, when sufficiently large voltage is applied (of order 1 Volt) often currents beyond I_{lim} are observed. Still unresolved are the mechanisms behind currents above the theoretical diffusion limit, referred to as the overlimiting current.

An electrohydrodynamic instability as a mechanism for overlimiting current (OLC) was first rigorously tested by Rubinstein *et al.* (1988), who measured I-V curves for several different cation selective membranes and related the excess noise to the appearance of the electro-osmotic instability (EOI). EOI refers to the experimentally observed vortices which arise in these systems. These vortices enhance the advective transport of salty solution across the depleted diffusion layer to the ion-selective membrane leading to increased current through the system. An abundance of additional experimental work has been carried out, such as that by Maletzki *et al.* (1992), who applied an immobilizing gel on the ion-selective membrane and showed the disappearance of OLC, presumably due to suppression of EOI.

More recently, the advent of micro- and nanofluidics has provided a new platform for the study of ion transport into ion-selective media (Chang *et al.* 2012) and chaotic electrohydrodynamic low Reynolds number flows (Posner *et al.* 2012). Recent studies using

micro- and nanofludic technology have made direct observations of the EOI vortices; Kim *et al.* (2007, 2012) at the interface between a microchannel and an array of nanochannels, Yossifon & Chang (2008) at the interface of a microchamber and a nanoslot, Rubinstein *et al.* (2008) at the interface of a microchamber and an ion-selective membrane, and Kwak *et al.* (2012) in a microfluidic electrodialysis cell.

Theoretical work on EOI has primarily used asymptotic theory in which the electrically charged boundary layer at the ion-selective membrane is approximated by a slip condition on the fluid. Several authors have contributed to the analysis of the complex structure of the electrochemical boundary layer (Chu & Bazant 2005; Yariv 2009). The analysis shows the appearance of a so-called extended space charge layer (ESC) at currents approaching the diffusion limit. Based on this ESC, Rubinstein & Zaltzman (2001) and Zaltzman & Rubinstein (2007) developed an effective slip condition modeling the boundary layer, thus eliminating the need to resolve it. Using this slip approximation, Rubinstein & Zaltzman (2000) and Rubinstein *et al.* (2008) were the first to carry out theoretical and numerical studies in the limit of a thin boundary layer and an electroneutral outer region. Follow-up studies have since been performed (Schiffbauer *et al.* 2012; Kalaidin *et al.* 2012). In all these studies, the appearance of EOI has been shown in the form of arrays of vortex pairs on the ion-selective membrane. However, from these studies it is unclear to what degree this slip approximation correctly captures all the essential effects. Recent calculations have shown that rather non-intuitive chaotic modes exist due to interactions between the flow and electrostatic forces (Demekhin *et al.* 2008; Shelistov *et al.* 2011; Demekhin *et al.* 2011; Pham *et al.* 2012).

Finally, other mechanisms have been suggested as routes for OLC including surface conductance in microchannels (Dydek *et al.* 2011) and the chemical mechanism of current-induced membrane discharge (Andersen *et al.* 2012). These mechanisms may act in concert with EOI. For now we leave a combined study of these effects with EOI for future work.

We have recently developed numerical tools for direct simulation of ionic transport coupled with flow and electrostatic forces near ion-selective surfaces. In particular, our calculations use a low Reynolds number approximation and ignore the inertial terms in the Navier–Stokes equations. We show that such a model can consistently predict chaotic EOI for systems sustaining OLC. Furthermore, our calculations predict strong advection with time scales competing with the charge relaxation time. As a result, the EOI vortices can cause the otherwise thin space-charge regions on the surface to be ejected into the bulk of the domain and result in complex dynamic interactions between the flow and electrostatic forces. We present results from spectral analysis of these flows and show that they resemble signals from inertial turbulent flows.

2. Model system

We consider a two-dimensional model domain of length L in the $\tilde{x}$-direction and width $\tilde{w}$ in the $\tilde{y}$-direction as shown in Figure 1. In our notation, a dimensional quantity carries a tilde only if it has a dimensionless representation. The domain considered in Figure 1 corresponds to a semi-empirical boundary region between a reservoir of uniform properties and an ion-selective membrane. The domain is filled with a binary, symmetric and inert electrolyte of mass density ρ, viscosity μ, and electrical permittivity ε. The two ionic species have a diffusion coefficient D and valence z. The domain boundary at $\tilde{x} = 0$ corresponds to the ion-selective membrane which is assumed cation-selective, i.e., freely

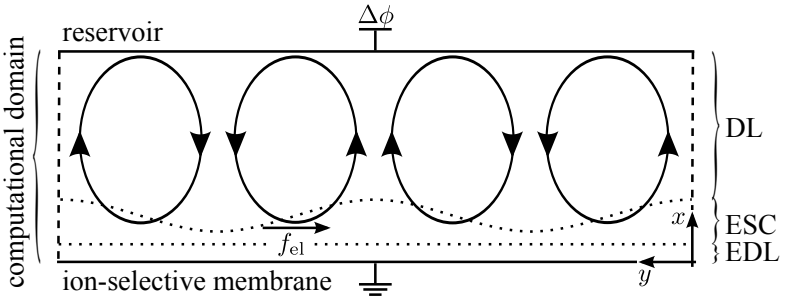

FIGURE 1. The model domain (not to scale).

permeable to cations and impenetrable to anions. Additionally, the electrolyte fluid has zero slip on the membrane surface, and the electric potential is grounded at this surface. The domain boundary at $\tilde{x} = L$ corresponds to a reservoir of ionic concentration c_0 and with an applied electric potential of $\Delta\tilde{\phi}$. At this boundary the hydrodynamic pressure is zero, and the boundary condition for the velocity field corresponds to typical far-field conditions, i.e., tangential velocity is zero and the normal gradient of the normal velocity is zero. Periodic boundary treatments are employed in the $\tilde{y}$-direction.

3. Governing equations

Conservation of momentum is described by the Navier–Stokes equation in which the inertial term $\rho \mathrm{D}\tilde{\boldsymbol{v}}/\mathrm{D}\tilde{t}$ is neglected,

$$\boldsymbol{0} = -\tilde{\boldsymbol{\nabla}}\tilde{p} + \mu\tilde{\nabla}^2\tilde{\boldsymbol{v}} - \tilde{\rho}_e\tilde{\boldsymbol{\nabla}}\tilde{\phi}, \tag{3.1}$$

where $\tilde{\boldsymbol{v}} = \tilde{u}\,\hat{\boldsymbol{x}} + \tilde{v}\,\hat{\boldsymbol{y}}$ is the velocity vector field, $\tilde{p}$ is the pressure, $\tilde{\rho}_e$ is the electric charge density, and $\tilde{\phi}$ is the electrostatic potential. The fluid is incompressible whereby the continuity equation applies,

$$\tilde{\boldsymbol{\nabla}} \cdot \tilde{\boldsymbol{v}} = 0. \tag{3.2}$$

Gauss's law relates the electrostatic potential and the electric charge density

$$-\varepsilon\tilde{\nabla}^2\tilde{\phi} = \tilde{\rho}_e = ze\left(\tilde{c}^+ - \tilde{c}^-\right), \tag{3.3}$$

where $\tilde{c}^+$ and $\tilde{c}^-$ are the cationic and anionic concentration field, respectively, and e is the elementary charge. Mass conservation of the two ions is expressed by the equation

$$\frac{\partial\tilde{c}^{\pm}}{\partial\tilde{t}} = -\tilde{\boldsymbol{\nabla}} \cdot \tilde{\boldsymbol{j}}^{\pm}, \tag{3.4}$$

in which the ionic mass flux $\tilde{\boldsymbol{j}}^{\pm}$ is given by the Nernst–Planck equation in terms of diffusion, electromigration and advection,

$$\tilde{\boldsymbol{j}}^{\pm} = -D\tilde{\boldsymbol{\nabla}}\tilde{c}^{\pm} \mp D\frac{ze}{k_{\mathrm{B}}T}\tilde{c}^{\pm}\tilde{\boldsymbol{\nabla}}\tilde{\phi} + \tilde{c}^{\pm}\tilde{\boldsymbol{v}}, \tag{3.5}$$

where k_{B} is the Boltzmann constant and T is the temperature.

3.1. *Dimensionless equations*

We scale time by the diffusion time t_0, position by the surface-to-reservoir length L, velocity by the diffusion velocity v_0, concentration by the reservoir concentration c_0,

pressure by the osmotic pressure p_0, electric potential by the thermal voltage V_T, and ionic flux by the diffusion flux j_0,

$$t_0 = \frac{L^2}{D}, \quad v_0 = \frac{D}{L}, \quad p_0 = \frac{\mu D}{L}, \quad V_\mathrm{T} = \frac{k_\mathrm{B}T}{ze}, \quad j_0 = \frac{Dc_0}{L}, \tag{3.6}$$

to obtain the dimensionless variables,

$$t = \frac{\tilde{t}}{t_0}, \quad \boldsymbol{x} = \frac{\tilde{\boldsymbol{x}}}{L}, \quad \boldsymbol{v} = \frac{\tilde{\boldsymbol{v}}}{v_0}, \quad c^\pm = \frac{\tilde{c^\pm}}{c_0}, \quad p = \frac{\tilde{p}}{p_0}, \quad \phi = \frac{\tilde{\phi}}{V_\mathrm{T}}, \quad \boldsymbol{j}^\pm = \frac{\tilde{\boldsymbol{j}}^\pm}{j_0}. \tag{3.7}$$

The non-dimensional Navier–Stokes and continuity equations are

$$\mathbf{0} = -\boldsymbol{\nabla} p + \nabla^2 \boldsymbol{v} - \frac{Pe}{2\epsilon^2}\left(c^+ - c^-\right)\boldsymbol{\nabla}\phi, \tag{3.8}$$

$$0 = \boldsymbol{\nabla}\cdot\boldsymbol{v}, \tag{3.9}$$

where the neglected inertial term is $(1/Sc)\mathrm{D}\boldsymbol{v}/\mathrm{D}t$ in which the Schmidt number $Sc = \mu/(\rho D)$ is typically $O(10^3)$. The material Peclet number,

$$Pe = \frac{\varepsilon}{\mu D}\left(\frac{k_\mathrm{B}T}{ze}\right)^2 \tag{3.10}$$

is typically $O(1)$. The dimensionless screening length of electric charge,

$$\epsilon = \frac{\lambda_\mathrm{D}}{L}, \tag{3.11}$$

is typically much smaller than unity $\epsilon \ll 1$ and defined in terms of the Debye–Hückel screening length,

$$\lambda_\mathrm{D} = \sqrt{\frac{\varepsilon k_\mathrm{B}T}{2(ze)^2 c_0}}, \tag{3.12}$$

which is inversely proportional to the square-root of concentration. A common concentration $c_0 \sim O(100\ \mathrm{mM})$ results in $\lambda_\mathrm{D} \sim O(1\ \mathrm{nm})$, which for a typical $L \sim O(100\ \mu\mathrm{m})$ yields $\epsilon \sim O(10^{-5})$. The non-dimensional Gauss's law,

$$-2\epsilon^2\nabla^2\phi = c^+ - c^-, \tag{3.13}$$

illustrates mathematically the formation of the electric double layer (EDL) at charged surfaces as the small parameter ϵ multiplies the highest derivative. As already mentioned, the smallness of ϵ has been used for singular asymptotic analyses to derive fluid-slip models for the electrically induced flow on ion-selective membranes. Such asymptotic models simplify the governing equations and the numerical complexity of EOI, but their assumption that the flow does not significantly affect the boundary layer structure is not accurate. One aim of this work is to investigate in full detail the structure of the boundary layer in the presence of EOI. Finally, the dimensionless ion mass conservation and Nernst–Planck flux,

$$\frac{\partial c^\pm}{\partial t} = -\boldsymbol{\nabla}\cdot\boldsymbol{j}^\pm, \tag{3.14}$$

$$\boldsymbol{j}^\pm = -\boldsymbol{\nabla}c^\pm \mp c^\pm\boldsymbol{\nabla}\phi + c^\pm\boldsymbol{v}, \tag{3.15}$$

introduce no additional dimensionless parameters.

3.2. *Boundary and initial conditions*

On the membrane boundary at $x = 0$, there is no-slip, a grounded potential, a fixed cation concentration and no-flux condition for anions,

$$\boldsymbol{v} = \mathbf{0}, \qquad \phi = 0, \qquad c^+ = 2, \qquad j_x^- = 0, \tag{3.16}$$

while on the reservoir boundary at $x = 1$, there is a fully developed flow, zero pressure, an applied potential $\Delta\phi$, and fixed cation and anion concentration,

$$\frac{\partial u}{\partial x} = 0, \qquad v = 0, \qquad p = 0, \qquad \phi = \Delta\phi, \qquad c^+ = c^- = 1. \tag{3.17}$$

Finally, we employ periodic boundary conditions between the boundaries at $y = 0$ and $y = w$.

The initial condition is generated by extruding into 2D the result from a corresponding 1D quiescent model and randomly perturbing the concentration fields in each grid point by 1 %. With this method we avoid the numerical cost associated with a 2D computation of the initial stage of the concentration polarization process. This has no effect on the long-time statistics of the dynamics, but it could have an impact on the transition process from the quiescent state to the EOI state.

3.3. *Computational details*

The mesh is non-uniform in the x-direction and uniform in the y-direction. Thus, the mesh resolves the EDL and ESC boundary layers in the x-direction normal to the surface by a second-order central finite-difference scheme while numerical cost is saved by employing a spectral method in the lateral y-direction. The total number of mesh points in the x- and y-direction is 120 and 240, respectively, with the minimum and maximum x spacing as 7.7×10^{-4} and 1.7×10^{-2}, respectively. The length of the domain in the y-direction is $w = 8$. The time step is $\Delta t = 10^{-6}$ and the time integration for the ionic concentration fields is semi-implicit. Transport in the y-direction and the advective terms are treated explicitly, whereas the wall-normal electromigration and diffusion are treated implicitly. Potential, pressure, and the velocity fields are solved at each time step using a direct solver utilizing Fourier transforms in the y-direction and banded matrices in the x-direction.

4. Basic physical picture of EOI

Before proceeding we give a basic physical explanation of the positive feedback in EOI. Figure 1 shows a sketch of EOI consisting of a periodic array of counter-rotating vortices. Studies of the system in the 1D quiescent case show that in the wall-normal direction the domain is electrochemically characterized by several distinct regions, three of which we consider here (Chu & Bazant 2005; Zaltzman & Rubinstein 2007; Yariv 2009). Closest to the surface is the thin EDL of thickness $O(\epsilon)$, which is related to classical electro-osmotic flow but cannot be responsible for EOI (Zaltzman & Rubinstein 2007). Just beyond the EDL is the ESC where concentration and charge density are both of $O(\epsilon)$. Finally, beyond the ESC is the approximately electroneutral diffusion layer (DL) of space charge $O(\epsilon^2)$ and in which the concentration varies from $O(1)$ at the reservoir to $O(\epsilon)$ at the DL-ESC interface (Yariv 2009).

As indicated in the figure, a positive feedback mechanism can be envisioned in which a tangential electric force drives a test vortex. This vortex generates additional concentration gradients: at the outflow position low concentration $c \ll 1$ flows towards the

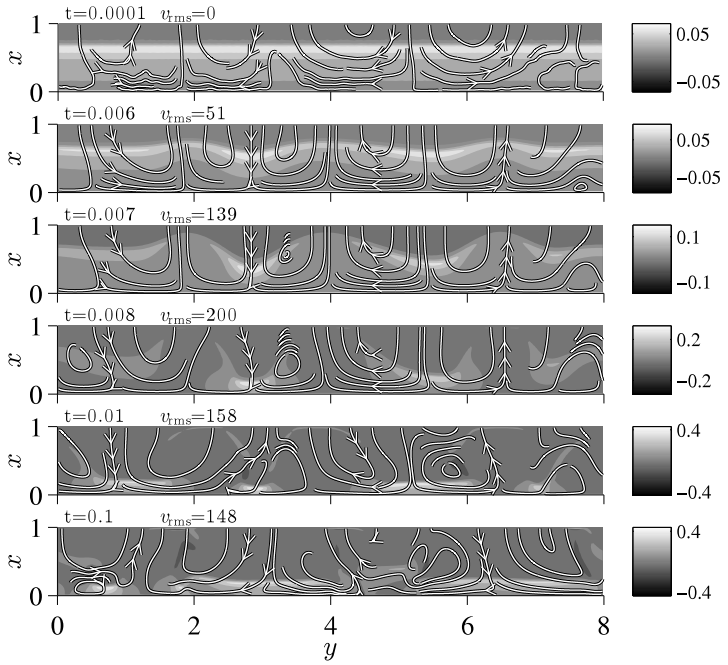

FIGURE 2. 2D contour plots of charge density (white and black color corresponding to negative and positive values, respectively) with flow lines superimposed at different times.

reservoir while at the inflow position high concentration $c \approx 1$ flows towards the membrane. This in turn leads to a higher and lower current density, respectively, at the inflow and outflow positions. As shown by Zaltzman & Rubinstein (2007), the change in current density perturbs the ESC generating an electric force density $\boldsymbol{f}_{\rm el}$ acting on the flow in the direction from the inflow to the outflow position. Thus, the test vortex enhances itself and the result is EOI in the form of an array of vortex pairs (Zaltzman & Rubinstein 2007). At sufficiently high currents the system becomes chaotic, and the slip-model assumption that the 1D quiescent structure of the ESC is unaffected by the flow is dubious. In any case, the advective transport by EOI of high-concentration electrolyte to the surface is what facilitates OLC.

5. Results

The following results are for a dimensionless screening length of $\epsilon = 10^{-2}/\sqrt{2}$. Figure 2 shows $\Delta\phi = 120$ snap shots at times $t = 0.0001$, 0.006, 0.007, 0.008, 0.01 and 0.1 of the charge density with flow lines superimposed. The RMS value of the velocity is given for each snap shot. At $t = 0.0001$, the charge density is still largely in its 1D quiescent state; the EDL is too small to distinguish at the boundary at $x = 0$, whereas the ESC is clearly visible extending more than half way to the reservoir boundary at $x = 1$. The flow has a small $v_{\rm rms} < 1$ magnitude, but a clear pattern has emerged of alternating inflow and outflow regions; as discussed above, these vortex structures have a positive feedback on themselves and will grow in time to develop EOI. At $t = 0.006$, the charge density is clearly perturbed by a moderately strong flow of $v_{\rm rms} = 51$ showing a lateral wavelength ≈ 2.5 of the perturbation. Since the vortices come in pairs of two, this corresponds to a lateral size of a single vortex of $O(1)$, i.e., on the order of the surface-to-reservoir distance.

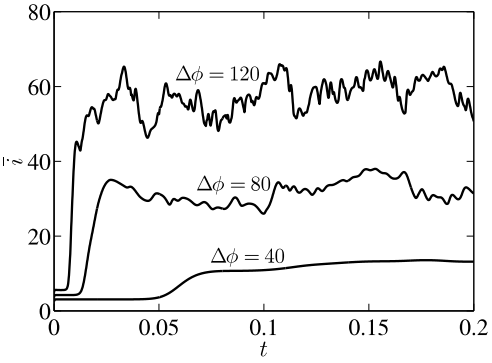

FIGURE 3. Area-averaged current density $\bar{i}$ versus time.

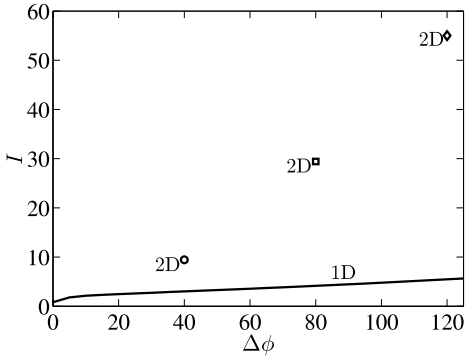

FIGURE 4. Time and area-averaged current density I versus applied voltage $\Delta\phi$ based on the 1D quiescent model (full curve) and on the 2D model (three symbols).

Furthermore, we see evidence of the basic physical picture of EOI; as the flow alternates between inward and outward as one traverses the y-direction, the ESC contracts and expands while the charge density increases and decreases. At $t = 0.007$ and 0.008, the increasing flow of $v_{\rm rms} = 139$ and 200 has made the perturbation grow and the periodicity of the lateral perturbation starts to break down. At $t = 0.01$, it appears that the flow has reached an oscillatory state as $v_{\rm rms}$ is smaller at 158, while regions of negative charge density have appeared and the structure of the ESC resembles mushrooms that appear to be coalescing. At $t = 0.1$, $v_{\rm rms}$ is again smaller at 148 and the charge density shows a complex structure without any apparent periodicity suggesting a chaotic state.

The area-averaged current density $\bar{i}$,

$$\bar{i} = \frac{1}{w}\int_0^w i_x \mathrm{d}y, \tag{5.1}$$

is plotted versus time in Figure 3 for three applied potentials $\Delta\phi = 40$, 80, and 120. The instability develops faster for larger applied potential with onset around $t = 0.05$, 0.02, and 0.01 for $\Delta\phi = 40$, 80, and 120, respectively. For $\Delta\phi = 40$, the current has no apparent high-frequency oscillations. For $\Delta\phi = 80$ and 120, high-frequency oscillations in the current are apparent, with the appearance of more higher frequencies for higher voltage.

Figure 4 shows as a function of the applied potential $\Delta\phi$ the time- and area-averaged current density I,

$$I = \frac{1}{\Delta t}\int_{t_0}^{t_0+\Delta t} \bar{i}\,\mathrm{d}t, \tag{5.2}$$

where t_0 is chosen after EOI has fully developed and Δt depends on the extent of the particular simulation. It is clear that the 2D model predicts OLC that are qualitatively in much better agreement with experimental observations when compared to the 1D quiescent model. Based on the three data points, the current in the OLC regime is seen to vary approximately linearly with applied potential.

Figure 5 shows for $\Delta\phi = 120$ the energy spectral density (ESD) for velocity component v at $x = 0.048$ as a function of the frequency ω of the temporal oscillations. The ESD is based on approximately 8000 time samples. The broadband structure of the ESD without

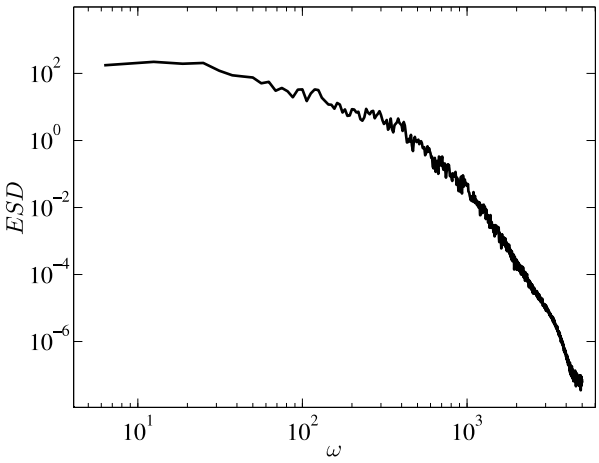

FIGURE 5. Energy spectral density (ESD) for velocity component v at $x = 0.048$ for $\Delta\phi = 120$ based on approximately 8000 time samples.

any peaks of periodic oscillations shows that the flow is chaotic.

6. Summary

We have solved numerically the full system of coupled transient Poisson–Nernst–Planck and Navier–Stokes equations at an ion-selective membrane for a dimensionless screening length of $10^{-2}/\sqrt{2}$ and applied potential up to 120 thermal voltage units. By computing the energy spectral density, we have shown that our model predicts chaotic electro-osmotic instability. Not only does this lead to over-limiting current, it is also a fundamental topic of interest since chaotic flows are not common in regimes of vanishing inertial effects.

To facilitate the DNS we have developed an efficient numerical scheme, taylored to handle the stiffness of the equations in the wall normal direction while saving computational cost for the transverse direction. The scheme is robust at high applied potential differences and is also suitable for extension to smaller screening lengths and thinner boundary layers.

Our results show that advection interacts strongly with the electrochemical boundary layers, changing their uniform quiescent state into a chaotic state. It appears that the asymptotic slip-condition (Rubinstein & Zaltzman 2001) is not valid in this case, and further DNS studies for smaller screening lengths are needed to clarify the validity of this approximation.

REFERENCES

ANDERSEN, M. B., VAN SOESTBERGEN, M., MANI, A., BRUUS, H., BIESHEUVEL, P. M. & BAZANT, M. Z. 2012 Current-induced membrane discharge. *Physical Review Letters* **109**, 108301.

CHANG, H.-C., YOSSIFON, G. & DEMEKHIN, E. A. 2012 Nanoscale electrokinetics and microvortices: How microhydrodynamics affects nanofluidic ion flux. *Annu. Rev. Fluid Mech.* **44**, 401–426.

Chu, K. T. & Bazant, M. Z. 2005 Electrochemical thin films at and above the classical limiting current. *SIAM J. Applied Mathematics* **65**, 1485.

Demekhin, E., Shapar, E. & Lapchenko, V. 2008 Initiation of electroconvection in semipermeable electric membranes. *Doklady Physics* **53**, 450–453.

Demekhin, E. A., Shelistov, V. S. & Polyanskikh, S. V. 2011 Linear and nonlinear evolution and diffusion layer selection in electrokinetic instability. *Physical Review E* **84**, 036318.

Dydek, E. V., Zaltzman, B., Rubinstein, I., Deng, D. S., Mani, A. & Bazant, M. Z. 2011 Overlimiting current in a microchannel. *Physical Review Letters* **107**, 118301.

Kalaidin, E., Tuguz, T. & Demekhin, E. 2012 Asymptotic solution of the Nernst-Planck-Poisson-Stokes set near a surface with selective properties. *Doklady Physics* **57**, 321–326.

Kim, S. J., Ko, S. H., Kwak, R., Posner, J. D., Kang, K. H. & Han, J. 2012 Multi-vortical flow inducing electrokinetic instability in ion concentration polarization layer. *Nanoscale* **4**, 7406–7410.

Kim, S. J., Wang, Y.-C., Lee, J. H., Jang, H. & Han, J. 2007 Concentration polarization and nonlinear electrokinetic flow near a nanofluidic channel. *Physical Review Letters* **99**, 044501.

Kwak, R., Guan, G., Peng, W. K. & Han, J. 2012 Microscale electrodialysis: Concentration profiling and vortex visualization. *Desalination* **308**, 138–146.

Levich, V. G. & Spalding, D. B. 1962 *Physicochemical hydrodynamics*. Prentice-Hall Englewood Cliffs, NJ.

Maletzki, F., Rösler, H.-W. & Staude, E. 1992 Ion transfer across electrodialysis membranes in the overlimiting current range: stationary voltage current characteristics and current noise power spectra under different conditions of free convection. *J. Membrane Science* **71**, 105–116.

Pham, V., Li, Z., Lim, K., White, J. & Han, J. 2012 Direct numerical simulation of electroconvective instability and hysteretic current-voltage response of a permselective membrane. *Physical Review E* **86**, 046310.

Posner, J. D., Prez, C. L. & Santiago, J. G. 2012 Electric fields yield chaos in microflows. *Proceedings of the National Academy of Sciences* **109**, 14353–14356.

Probstein, R. F. 1994 *Physicochemical Hydrodynamics: An Introduction*. John Wiley & Sons.

Rubinstein, I., Staude, E. & Kedem, O. 1988 Role of the membrane surface in concentration polarization at ion-exchange membrane. *Desalination* **69**, 101–114.

Rubinstein, I. & Zaltzman, B. 2000 Electro-osmotically induced convection at a permselective membrane. *Physical Review E* **62**, 2238.

Rubinstein, I. & Zaltzman, B. 2001 Electro-osmotic slip of the second kind and instability in concentration polarization at electrodialysis membranes. *Mathematical Models and Methods in Applied Sciences* **11**, 263300.

Rubinstein, S. M., Manukyan, G., Staicu, A., Rubinstein, I., Zaltzman, B., Lammertink, R. G. H., Mugele, F. & Wessling, M. 2008 Direct observation of a nonequilibrium electro-osmotic instability. *Physical Review Letters* **101**, 236101.

Schiffbauer, J., Demekhin, E. A. & Ganchenko, G. 2012 Electrokinetic instability in microchannels. *Physical Review E* **85**, 055302.

Shelistov, V., Nikitin, N., Ganchenko, G. & Demekhin, E. 2011 Numerical mod-

eling of electrokinetic instability in semipermeable membranes. *Doklady Physics* **56**, 538–543.

Yariv, E. 2009 Asymptotic current-voltage relations for currents exceeding the diffusion limit. *Physical Review E* **80**, 051201.

Yossifon, G. & Chang, H.-C. 2008 Selection of nonequilibrium overlimiting currents: Universal depletion layer formation dynamics and vortex instability. *Physical Review Letters* **101**, 254501.

Zaltzman, B. & Rubinstein, I. 2007 Electro-osmotic slip and electroconvective instability. *J. Fluid Mechanics* **579**, 173–226.